A Complete and Accurate Modular Numerical Computation Scheme for Multi-Coupled Electric Drive Systems

Martin Nell, Nora Leuning, Sebastian Mönninghoff, Benedikt Groschup,
Fabian Müller, Jan Karthaus, Markus Jaeger, Michael Schröder and Kay Hameyer

Institute of Electrical Machines (IEM), RWTH Aachen University
Schinkelstraße 4, 52062 Aachen, Germany
post@iem.rwth-aachen.de

***Abstract*—The accurate computation of multi-coupled electric drive systems is a complex process. In order to consider a variety of physical effects, their interactions as well as the interactions of different components, multiple fields of science have to be addressed. Numerical simulations help to compute these complex systems and to design machines in the best possible way for its specific application. The numerical computation scheme proposed in this paper consists of six main sectors: the rough machine design, the preparation of the finite element method including the characterization and modeling of materials, the electromagnetic simulation, the mechanical simulation, the control and power electronics and the thermal design and simulation. In each of the main sectors, different effects affecting the machine and the system behavior can be considered and calculated. Depending on the application they can be added or removed modularly in order to adapt the simulation effort and the simulation accuracy to the application. A detailed insight in the computation methods and approaches in each of these main sectors and their coupling is given in this paper.**

***Index Terms*—Machine Simulation, Numerical Computation, Electric Drive Systems, Rough Design, Mechanical Simulation, Electromagnetic Simulation, Control, Power Electronics, Thermal Simulation, Material Modeling, FEM Solver**

I. Introduction

The modeling of electric drive systems and electric machines is presented in many research and scientific publications. Various methods, approaches and models are used to calculate and simulate the behavior of an electrical machine. They differ in complexity, accuracy and computational effort. Since analytical models consider only a few physical effects, they are numerically effective but less accurate when compared to numerical or multi-coupled approaches [1]. The goal of analytical models is to gain a basic understanding of the machine and individual effects. The main goal of numerical as well as of multi-coupled simulations is to investigate the overall behavior of the electric drive system, including all physical effects. To represent all physical effects in a numerical simulation, three main conditions have to be fulfilled. First, the parameters describing the physical effect have to be known. Second, a coupling between the individual effects must be considered and third, a mathematical description of the effects must be implemented which converges numerically. Therefore, various engineering and scientific fields, such as electrical engineering and mechanical engineering, computer science, materials science, physics, mathematics or chemistry have to be covered.

Electric drive systems are used in a wide variety of applications and under a wide variety of requirements and boundary conditions. Their number in industry, households and mobility is constantly increasing. They vary from micro electrical machines to large powers, from low speed to high speed motors, from low torque to high torque and from low power to high power electric drive systems. In addition, electrical machines are integrated in a wide variety of environments, e.g. as in total artificial heart [2]. As a result, each design of an electrical machine is based on individual requirements and boundary conditions.

To design and very accurately simulate a machine, all physical effects and application requirements must be considered. Both aspects, on the one hand the different application requirements and on the other hand the exact description of all physical effects lead to a complex process of simulative and numerical design and calculation of electrical machines.

Depending on the application different requirements and boundary conditions, such as installation space, power, torque, voltage, current and temperature, are more crucial than others. For example traction drives have to have a high power density and a high efficiency at low-cost. The focus in household machines is often on the price and not on the efficiency. In the case of artificial hearts, the engine must first meet the vital requirements, such as a certain temperature limit, before the focus can be on efficiency and price. As a result, depending on the application and the electrical drive system it is not necessary to address every certain physical effect in the machine design process. An example is the effect of cutting edges. For a household machine, where an inexpensive manufacturing process mostly dominates the optimization of the efficiency, the effect of cutting edges to the efficiency is not of high interest. On the contrary, the effect of cutting edges to

the efficiency in traction drives will be of high interest due to the influence on the electric range. Therefore, it is proposed to use a modular numerical simulation and computation scheme. The modularity gives the possibility to design, compute and simulate an electric drive system by considering pre-selected effects and boundary conditions.

II. The Complete Modular Numerical Computation Scheme

The proposed complete modular numerical computation scheme for accurate multi-coupled electric drive systems in this paper is based on six sectors (Fig. 1).

Within each sector individual aspects can be added or removed modularly. The paper is structured according to the individual sectors. It begins with sector one, the rough design of the machine. Analytical models and empiric data are used to determine a first machine design considering the application requirements and boundary conditions. In the second sector the parameters describing the physical effects in the machine are studied. For this purpose, material measurements are performed and soft and hard magnetic material models are developed. Mathematical descriptions of the effects and the material models are implemented to the numerical solver and the machine geometries are prepared for a finite element (FE) simulation by meshing methods. The third sector, the electromagnetic simulation, is separated into two sub sectors. The first sub sector focus on the simulation of certain operating points and the effects of different physical effects such as cutting edges or flux barriers on the machine performance regarding different aspects such as acoustics or noise harshness and vibration (NVH). The second sub sector covers the simulation of the machine in their entire operating range. Operating diagrams describing the fluxes, voltages, currents, torques and further machine characteristics are calculated. A main focus in this sector is put to the loss power calculation, such as iron and Ohmic losses. Here, various information from the sectors before, such as the material parameters, are used. In addition scaling methods to scale the solutions of the FE simulation are applied. In the fourth sector, the mechanical design is performed and mechanical effects are simulated. For example, the influences of mechanical stress and the structural dynamic are analyzed as well as mechanical losses are computed. The fifth sector covers the aspects of the power electronics and control of the electrical drive system. With field coupling circuits the influences of the control and power electronics, e.g. by switched voltages, on the behavior of the machine are analyzed. Controllers are configured and control strategies are developed. In the sixth sector, thermal simulations are performed employing various models. Cooling concepts are developed and the temperature behavior of the machine is analyzed. In this process individual sectors can be coupled and have an influence on the other ones. The whole process is iterative.

III. Rough Design

The design of the machine starts with the rough design. In a first step the application requirements are analyzed. Fig. 2 shows the variety of contributing factors on the design of an electrical machine. From these contributing factors those are to be determined which have a limiting impact on the machine

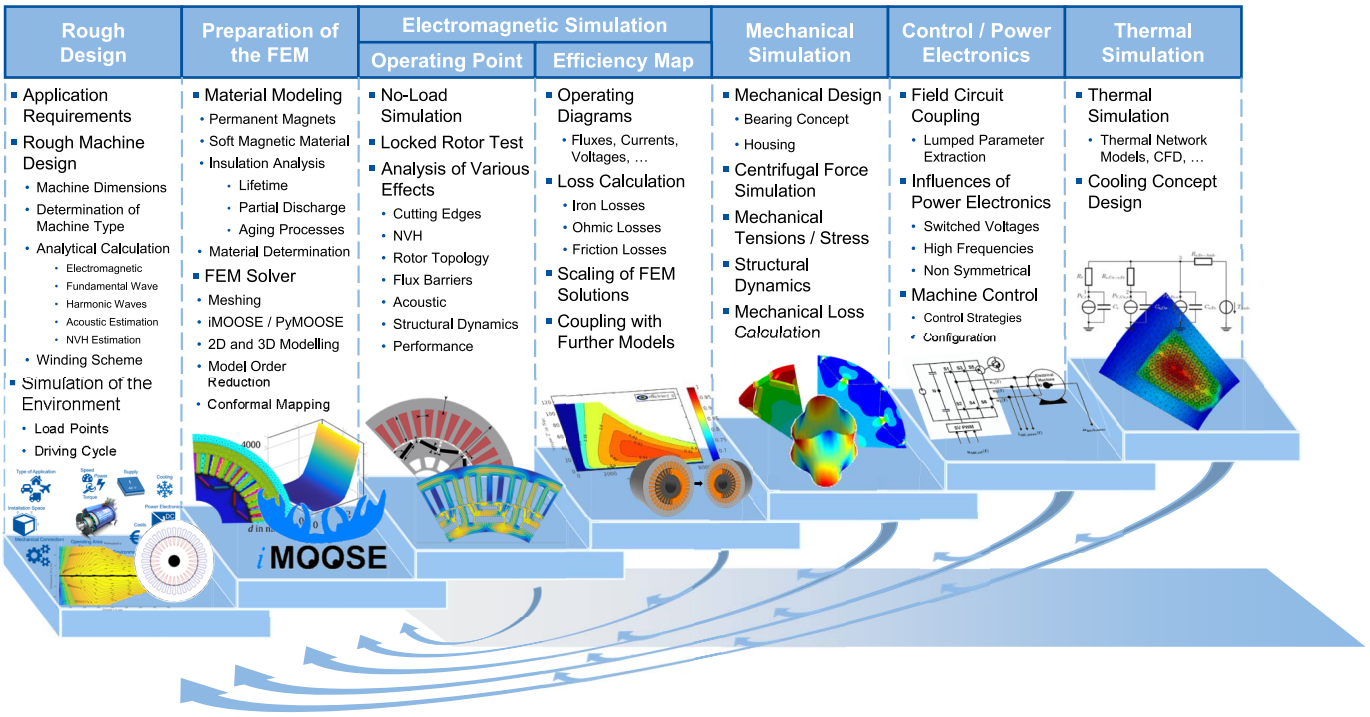

Fig. 1. IEM's modular numerical computation scheme of electric machines.

design, such as a given installation space. Electrical machines, especially traction drives, are often operated in many different operating points. For an appropriate design of the machine these operating points have to be known. Therefore, drive train simulations, such as vehicle simulation, are conducted using different driving cycles to get the speed, torque and power distribution of the machine [3]. The next step in the rough design process is the determination of the most suitable machine type for the given application. Different machine types such as the DC machine, the synchronous machine (SM), the reluctance machines (RM) or the induction machine (IM) have diverse advantages and disadvantages which have to be compared and to be evaluated to find the most suitable machine. An example of this process is discussed in [4].

The first rough design of the machine is calculated by using analytical formula. The input data of the analytic machine calculations are the analyzed information of the application and its requirements. In addition, first assumptions, such as Esson's number C_{mech} have to be made. The process of the rough machine design is separated in multiple steps. In the first step, the main dimensions of the machine are calculated. As an example, the bore diameter D of the machine can be calculated with the analyzed information and:

$$P_{\mathrm{mech}} = C_{\mathrm{mech}} D^2 l_{\mathrm{i}} n_{\mathrm{r}}, \tag{1}$$

where P_{mech} is the nominal mechanical power, l_{i} the active machine length and n_{r} the rated speed of the machine. In the second step, the winding is designed by using the air gap flux density, the nominal frequency and voltage and the speed as the input of the calculation. Furthermore, the magnetic equivalent circuit of the machine is drafted. For this step additional assumptions, which often are based on empirical data, are made. In the third step, the magnetic circuit is calculated. Hereby, it is possible to dimension the excitation winding for a SM or to calculate the magnetizing current of an IM. In the fourth step, the inductances and resistances of the machine are calculated, which are required to parameterize the electric equivalent circuit diagram. In the last step, the electric equivalent circuit diagram is used to determine the first loss and efficiency map. In addition to this process, further analytic methods can be used to get a first approximation about particular effects. One example is the analytic calculation of noise excitation, that helps to filter out unsuitable slot pole combination in an early step of the design process.

The rough design can not consider each physical effect but gives a good first evaluation of the machine design. Therefore, the results of the rough design are used in the further steps of the numerical computation scheme to enhanced the obtained results.

IV. Principle of Finite Element Method

The magnetic flux density in the air gap between the rotor and stator generates the torque of an electrical motor. The resulting torque is a direct consequence of the magnetization behavior of the ferromagnetic core material, which guides and increases the magnetic flux within the machine. For the

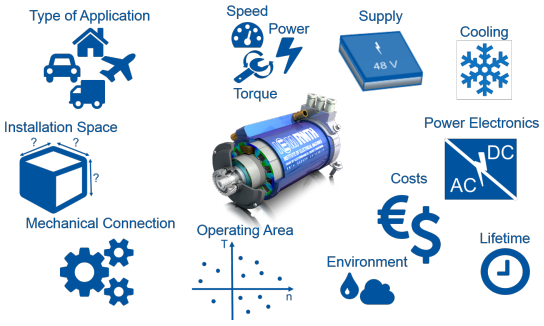

Fig. 2. Application requirements - contribution factors.

finite element method (FEM), the material behavior has to be portrayed as accurately as possible in order to estimate the magnetic field distribution locally. The magnetic material in the FEM is determined with the help of its reluctivity and conductivity. Apart from the magnetizing behavior, the generated losses are the next fundamental quantity of interest for the analysis of electrical machines. On the one hand, the copper losses from the windings and on the other hand the iron losses connected to the frequency and speed of the machine from the electrical steel.

Due to the non-linear behavior, local saturation and complex geometries, analytical tools are not sufficiently accurate to analyze the operational characteristics. In order to analyze the operational characteristics of the machine, the FEM is utilized. Material models in combination with adequate meshing, the consideration of model related convergence requirements and acceptable computational effort are used to predict the machine behavior. Due to the improvements in physical understanding of detrimental effects and a more detailed observation of the magnetic behavior, advanced material models are the focus of various research. However, these models have to be implemented into the FE environment and meet the specific requirements. In the following section, the basics of the FEM and material modeling are presented. A differentiation between

1) Pre-processing: Meshing, reluctivity
2) Processing: FEM solving with iMOOSE/pyMOOSE
3) Post-processing: Iron-loss modeling

has to be made in order to understand the relations, model coupling and recent advancements in the electromagnetic simulation of electrical machines.

1) Meshing: A first step of the pre-processing for the FEM is the meshing, where the geometry is discretized into sub domains, i.e. elements, which are connected by nodes. The accuracy that can be acquired from any FE model is directly associated with the FE mesh. For 2-D analysis, the elements are 2-D triangles, whereas for 3-D analysis, the elements have tetrahedral shape. Mesh refinement is an essential step in validating the FE model. Reducing the element size is the easiest mesh refinement strategy. The mesh size affects for example corners artifacts. The more elements are used the more computational effort it requires. However, different regions can be modeled with different mesh sizes without loosing

vital information, e.g. different mesh sizes for electrical steel, surrounding air or windings.

2) FEM solver: The FE library iMOOSE, developed since many years at the Institute of Electrical Machines (IEM), is a comprehensive tool for the design process, the analysis and optimization of electrical machines. Novel material models and solver can be easily implemented in the FE environment and thereby advance the numerical simulation of electrical machines steadily. Static as well as transient two- and three-dimensional electromagnetic problems can be modeled with iMOOSE considering the relative motion between stator and rotor. Additionally included is a harmonic problem solver with nonlinear material properties. By defined interfaces iMOOSE is coupled to the interpreter language Python (pyMOOSE) for rapid solver prototyping.

finite element analysis (FEA) of electromagnetic problems is generally based on the principles of the four Maxwell equations in combination with the constitutive laws for the magnetic flux density $\vec{B}$, electrical current density $\vec{J}$ and the electrical flux density $\vec{D}$. For the numerical simulation of electrical machines, either the magneto static formulation (MSF) in case of static simulations or the quasi magneto static formulation (QMSF) for transient simulations can be used to calculate the magnetic fields within the geometry, with solving starting from a Newton-Raphson approach considering all boundary conditions in the entire solving space. In iMOOSE/pyMOOSE the magnetic vector potential $\boldsymbol{A}$ or the magnetic scalar potential can be utilized. The magnetic vector potential is a function of place and time and given in (2),

$$\boldsymbol{B} = \nabla \times \boldsymbol{A}. \tag{2}$$

In state-of-the-art FEM, the static formulation is a combination fo the Ampère law and the constitutive law of the magnetic field,

$$\nabla \times (\nu \boldsymbol{B}) = \boldsymbol{J} + \frac{\partial \boldsymbol{D}}{\partial t}, \tag{3}$$

$$\nabla \times (\nu \nabla \times \boldsymbol{A}) = \boldsymbol{J} + \frac{\partial \boldsymbol{D}}{\partial t}. \tag{4}$$

In this formulation, ν can either be a scalar or a tensor, and describes the reluctivity of the material. This reluctivity describes the non-linear magnetic behavior of the flux density $\boldsymbol{B}$ and thereby is the crucial formulation to represent material behavior in the FEM. Usually due to low frequencies the displacement current density can be neglected.
The magnetic scalar potential formulation origins from a scalar potential Ω in combination with an exciting electric vector potential T:

$$\boldsymbol{H} = \boldsymbol{T} - \nabla \boldsymbol{\Omega}. \tag{5}$$

The electric vector potential is the sum of a potential T_0, which is produced by the windings, and a eddy current driven potential T_e. Substituting (5) into the material equation and in Faraday's law results in an accurate magneto dynamic formulation which can be combined with non conformal motion by Lagrange multipliers [5]:

$$\nabla \times (\frac{1}{\sigma} \nabla \times \boldsymbol{T}_\mathrm{e}) + \frac{\partial \mu \boldsymbol{T}_\mathrm{e} - \partial \mu \nabla \Omega}{\partial t} = -\frac{\mu \partial \boldsymbol{T}_0}{\partial t}, \tag{6}$$

$$\nabla \cdot (\mu \boldsymbol{T}_\mathrm{e}) - \nabla \cdot (\mu \nabla \Omega) = -\nabla \cdot (\mu \boldsymbol{T}_0). \tag{7}$$

Assembling the weak form of these differential equations leads to a system of linear equation, which needs to be solved with reasonable solvers for e.g. a conjugate gradient procedure.

3) Reluctivity: It is the soft magnetic materials reluctivity, which grants the analysis of the material's magnetization behavior in the FEM. In standardized simulations, the highly non-linear material behavior can be described with the help of the scalar reluctivity ν according to (8) as a function of B^2. The measurement of magnetization curves at a certain frequency provides the necessary information of the magnetic field strength H and the magnetic flux density B,

$$\nu = \frac{H}{B}. \tag{8}$$

Due to numerical requirements, the slope of the graph has to be positive (9), in order to enable a distinct attribution of ν to B, that is unambiguous,

$$\frac{\partial \nu}{\partial B^2} > 0. \tag{9}$$

Another requirement from the FEM is the extrapolation of the reluctivity curve up to several Tesla to avoid a possible break down of the simulation due to convergence. Magnetic measurements are often, due to the setup, limited to 1.8 T to 1.9 T. By means of extrapolation methods, for example the Fröhlich-Kenelly extrapolation, the $H - B$ characteristics can be extrapolated (10). The reluctivity can be extrapolated. Above the saturation the magnetic flux density B increases just by the value of $\mu_0 H$:

$$B = \mu_0 H + M_s. \tag{10}$$

In Figure 3 (a) the current state-of-the-art representation of reluctivity is depicted. However, advanced material models are subject of recent developments to improve FE machine simulations, due to the advanced physical understanding of occurring effects. One example for such an advancement is the continuous local material model to consider cut-edge effects of electrical steel laminations. The magnetic property deterioration due to cutting is significant and should not be neglected [7], [8]. Recent studies suggest that the losses increase in the range of 30 % when cutting is considered [9]. The model presented in [10] describes the local permeability $\mu_\mathrm{r}(x)$ as a function of the undamaged permeability $\mu_{\mathrm{r,\,u}}$, the local deterioration profile $\eta(x)$ and the maximum permeability drop at the cut surface $\delta\mu_\mathrm{cut}$:

$$\mu_\mathrm{r}(x) = \mu_{\mathrm{r,\,u}}(H) - \eta(x) \cdot \delta\mu_\mathrm{cut}(H). \tag{11}$$

Thereby, the magnetic flux in variable distance x from the

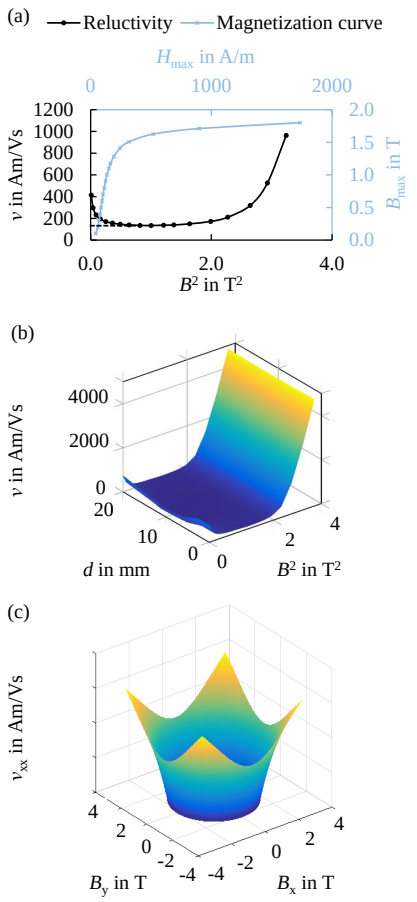

Fig. 3. (a) Reluctivity and (b) considering cut edge effect [6] and (c) simulation with magnetic anisotropy.

cut edge can be determined by

$$J(H,x) = (\mu_0 \cdot H\,(\mu_{\mathrm{r,u}}\,(H) - \Delta\mu_{\mathrm{cut}}\,(H) \cdot \eta\,(x)))\,\mathrm{d}x, \quad (12)$$

which then can be used to calculate the reluctivity. This can be used to create a reluctivity surface, as depicted in Figure 3 (b), where d is the distance to the closest cut-edge. In order to use the continuous material model in FE simulations an algorithm needs to assign the minimum distance to the cut surface for each element. The distance of the element to the cutting edge is stored as additional property of the mesh element. An example of a simulation with and without the consideration of cutting is depicted in Figure 4 from [11]. In this case, the difference between the simulation with damage compared to the undamaged case is locally up to 0.5 T.

Another effect that can be considered is the anisotropy of the material characteristics. The reluctivity ν is generally, a strict positive semidefinite tensor. In the case of isotropic materials, this tensor is reduced to a tensor without side entries and the same value on the main diagonal, i.e. equal to a scalar. Thus, it is restricted to isotropic material consideration. In reality however, even non-oriented electrical steels have a magnetic anisotropy. Not only does this magnetization anisotropy depend on the crystallographic texture and can have hardest

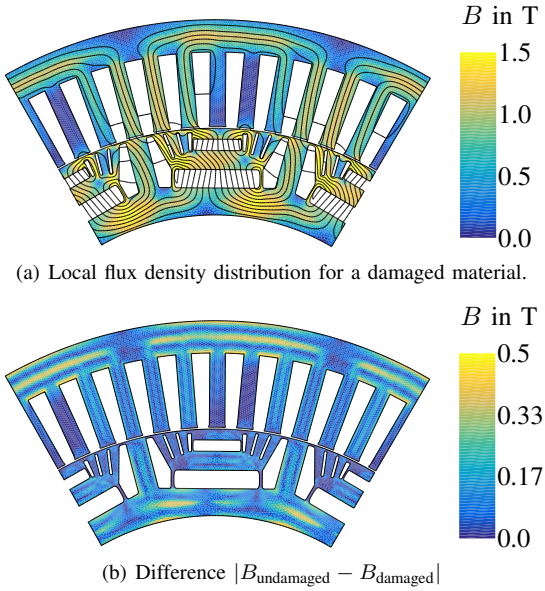

(a) Local flux density distribution for a damaged material.

(b) Difference $|B_{\mathrm{undamaged}} - B_{\mathrm{damaged}}|$

Fig. 4. Example for the local flux density distribution considering the cut edge effect, (a) local flux density (b) total difference between undamaged and damaged simulation at one operating point [11].

magnetization directions not only in transverse direction but, also in other directions, there is also a phase shift θ_{BH} between the magnetic field and the magnetic flux.

The scientists of the IEM develop model approaches to represent the material behavior including the information about the vector relationship between magnetic flux density excitation B and corresponding magnetic field H. An example for one of the derived entities of the reluctivity tensor for ν_{xx} is depicted in Figure 3 (c).

4) Loss modeling: Besides the magnetization behavior and local flux density distribution, the other crucial quantity for the analysis of electrical machines are the losses. The estimation of iron losses of soft magnetic materials can be conducted with different loss models. In the presented machine simulation regime, the calculation and determination of the loss distribution is placed to the post-processing of the FE solution. Nevertheless, the loss model has to be in line and coherent with the FEM.

Classical loss models can be distinguished in empirical and physical approaches. An example for empirical models is the Steinmetz equation:

$$P_{\mathrm{Steinmetz}} = k f^{\alpha} \hat{B}^{\beta}, \quad (13)$$

which is solely based on a fit of measurement data from various frequencies and inductions. It is based on an equation proposed by Steinmetz, which at one point was formulated without the frequency dependence of today's version [12]. This loss model is limited to sinusoidal waveforms and, due to the empirical nature strongly dependent on the number of measurements.

Another problem with this equation is the extrapolation to higher frequencies, because it suffers from poorer ac-

curacy compared to more physically motivated approaches. Comprehensive measurement data over the entire polarization range is often available only at frequencies lower 750 Hz up to 1000 Hz. For application of higher frequencies or the consideration of higher harmonics, the losses need to be taken into account at frequencies above 1000 Hz. Another strong drawback considering advanced FEM approaches is the interpretation of results compared with structural materials parameters. Material thickness, grain size or crystallographic texture affects the frequency dependence [13]. By variation of these parameters materials can be optimized for certain applications, for example frequencies. Thus, advanced loss models need to be used to allow a correlation of material parameters to different loss components. One of the commonly used loss models is the so-called Bertotti model:

$$P_{\text{Bertotti}} = k_{\text{hyst}}\hat{B}^{\alpha}f + k_{\text{cl}}B^2f^2 + k_{\text{exc}}B^{1.5}f^{1.5}, \tag{14}$$

which represents a physically motivated loss calculation. In this model, the total losses are the sum of hysteresis losses P_{hyst}, classical eddy current losses P_{cl} and the excess losses P_{exc}. Each loss component is linked to a different physical origin, i.e. the Barkhausen jumps, global eddy current and local eddy currents in the region of domain wall movements. In the model k_{hyst}, k_{cl}, k_{exc} and α are parameters that can be deduced by magnetic measurements and material parameters such as, thickness, electrical resistivity and specific density.

A general strength of the Bertotti model is its comprehensive physical explanation. However, the estimation of losses at high frequencies and inductions is a significant drawback. In [14] and [15] it is shown that the classical Bertotti model underestimates losses at high magnetic flux densities and high frequencies. In [14] the IEM Formula is introduced, which takes the Bertotti model but adds an additional term, called saturation loss to the loss equation to account for the non-linear material behavior. This results in the mathematical formulation:

$$\begin{aligned} P_{\text{IEM}} =& a_1\hat{B}^{\alpha+\hat{B}\beta}f + a_2\hat{B}^2f^2 \\ &+ a_2a_3\hat{B}^{2+a_4}f^2 + a_5(\hat{B}f)^{1.5}. \end{aligned} \tag{15}$$

The IEM-Formula shows improvement in loss determination at high magnetic flux densities and high frequencies, due to this fourth loss term with a higher order $\hat{B}$ dependence [16]. In various scientific studies, this model has been used to calculate the losses in electrical machines. It can be combined with the continuous local cut-edge model or other variants, for example the general dependency of mechanical stress described in section VI [17]. In [13], the effect of texture and grain size on the iron loss components has been studied. Dependent on the application's requirements for the flux densities and frequencies, different materials can be chosen to optimize the electrical machines operational characteristics considering physical effects, e.g. cutting, based on FE simulations.

5) Model order reduction: Large scale FE models arise from e.g. time dependent electromagnetic field problems, due to the skin depths of the eddy currents. On the one hand, to properly model eddy currents, the conducting regions have to be accurately discretized in space. On the other hand the time interval has to be accurately sampled to consider transient effects. The resulting computational effort of these transient simulations can be reduced by model order reduction (MOR). The reduction techniques can be distinguished in two classes, namely a-posteriori and a-priori approaches. One well known a-posteriori method is the proper orthogonalized decomposition (POD), which is based on collecting snapshots of the reference system to calculate a reduced representation. A-priori methods such as the proper generalized decomposition (PGD) method construct a reduced order model without any previously obtained solutions [18]. Both methods are implemented in iMOOSE and are currently focus of research. The POD is based on the accumulation of reference solutions to extract crucial informations of the system. This procedure is called snapshot method. Afterwards a singular value decomposition of the collected vectors is done and utilized to create a projection $\boldsymbol{\Psi}$. The projection is further utilized to achieve a reduced linear system which is much smaller than the reference system. This procedure is not depending on the underlining differential equation. This leads to the fact that:

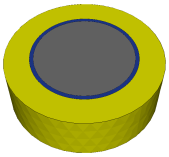

Fig. 5. Example geometry of an eddy current problem.

$$\mathbf{M}\boldsymbol{X} = \boldsymbol{B} \tag{16}$$

can be approximated by:

$$\boldsymbol{\Psi}^t\mathbf{M}\boldsymbol{\Psi}\boldsymbol{\Psi}^t\boldsymbol{X} = \boldsymbol{\Psi}^t\boldsymbol{B}. \tag{17}$$

In fact the reduced system has a dimension, which is equal to the number of snapshots taken from the reference system. This easily leads to a reduction of the degrees of freedom of several thousand leading to a much faster solving of the matrix system [19]. The PGD is based on another approach:

$$\boldsymbol{U} \approx \sum_{i=1}^{m} \mathbf{R}(x)S(t). \tag{18}$$

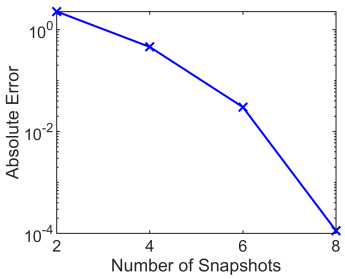

Fig. 6. Relative error of joule losses.

It assumes that the unknown vector field $\boldsymbol{U}$ can be decomposed into several functions, e.g. $\mathbf{R}(x)$ and $S(t)$, only depending on a single variable such as space x or time t [20].

6) Electrical insulation system: The winding system of electrical machines are currently not part of the electromagnetic FEA and not a directly coupled simulation routine. However, the phenomenological behavior of the insulating system is of important concern for recent developments of electrical machines. A trend for semi-conductors are rising switching frequencies and voltage slew rates in order to reduce the size of passive components of the electric circuit and to reduce switching losses. Life-time analysis considering thermal, thermo-mechanic or electric aging is studied and corresponding mathematical models are developed. Significant topics e.g. high du/dt inverter voltages and partial discharge (PD) phenomena in the insulation systems of low voltage drives. Progress in the characterization methods and insulation materials enable the modeling and consideration of winding system life-time for electrical machines [21], [22].

V. Electromagnetic simulation scheme

The analytic equations, describing the electromagnetic behavior of the machine, in the rough design process can only consider a few physical effects. To consider for example saturation and flux leakage effects or the effects of cutting edge or similar specific material impacts on the electromagnetic behavior of the machine a numerical electromagnetic FE simulation is necessary. In a first step the numerical FE simulations are conducted for single operating points. In the next step, the calculation of efficiency maps, the simulations are extended to the whole operating range of the machine. In the following, various simulation methods and approach are described.

A. Operating point simulation

With a **no-load simulation** the stator flux linkage and the back-emf of SMs are calculated. In addition, the magnetic flux distribution is visualized [23]. In the case of the IM this type of simulation is also used to extract the lumped parameter matrices that are necessary for the hybrid simulation scheme described in [24] and the next section.

The **demagnetization test** is used for permanent magnet machines (PM). With this simulation the overload capability of the machine geometry is determined [23]. In the worst case the maximum d-current is fed into the machine due to a fault in the power electronic. In this case the demagnetization is at its highest value and should not cause irreversible demagnetization.

The torque of a SM is defined by:

$$T = \frac{3p}{\omega} \left(U_\mathrm{p} - I_\mathrm{d} \cdot \left(X_\mathrm{q} - X_\mathrm{d} \right) \right) \cdot I_\mathrm{d}. \tag{19}$$

With $I_\mathrm{d} = I \cos(\Psi)$ and $I_\mathrm{q} = I \sin(\Psi)$ and the field weakening angle Ψ the torque is:

$$T = \hat{T}_\mathrm{syn} \cos(\Psi) - \hat{T}_\mathrm{rel} \sin(2\Psi). \tag{20}$$

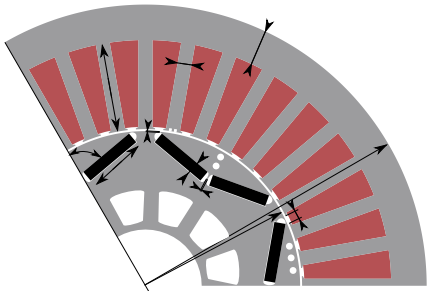

Fig. 7. Relevant parameters of the SM geometry.

The torque reaches its maximum value for the optimum field weakening angle Ψ_opt. To get the absolute value of the synchronous and reluctance torque, $\hat{T}_\mathrm{syn}$ and $\hat{T}_\mathrm{rel}$ respectively, as well as the optimum field weakening angle the **locked rotor test** is conducted. The locked rotor test is performed stepwise with increasing stator current density to determine the load dependency of those quantities [23]. By analyzing the load current and field weakening angle in the locked rotor test the L_d and L_q inductances of the SM are calculated. This parameters are necessary to determine the field weakening capability, the torque and the control of the machine.

In the **operating point simulation** certain interesting operating points are simulated. The goal of these simulations is to refine the geometry of the machine due to a better performance and to analyze specific impacts. An example of the analyzes of such specific impacts are the effects of flux barriers that are described in [25] or the effect of cutting edges onto the electromagnetic behavior, which is described in section IV and the scientific publications [26] and [27]. In the refinement process of the machine geometry, individual machine parameters or combinations of them are iteratively varied to find the best possible parameter combination for the given specification. Important geometrical manipulated variables are shown exemplary for the SM in Fig. 7. Evaluation criteria for the selection of favorable parameter combinations can be very different. Examples of evaluation criteria are the cogging torque, the torque ripples, the maximum torque, harmonics of the air gap field or the losses.
Application examples of this simulation method for geometry refinement were carried out in many scientific publications, such as [28], [29] and [30].

B. Efficiency map simulation

In addition to the simulation and analysis of specific operating points, the simulation and analysis of the entire operating range of the designed machine is also be conducted. This entire operation ranges are often of high interest if the machine operates not only in a few but in many different operating points such as it is for traction drives. Therefore, the simulation of the machine's losses, the Ohmic losses in the stator and the rotor, the friction losses and the iron losses in the stator and rotor in the entire operating range is the main goal in this step. With the simulated losses the efficiency map of the

machine can be determined. Figure 8 shows such an exemplary efficiency map for an IM. To calculate the losses the developed knowledge of the steps before, such as the iron loss models and their parameters in section IV, are used.

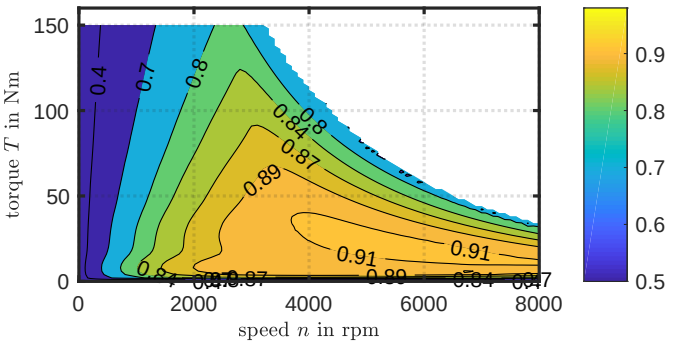

Fig. 8. Efficiency map of an IM.

DC machines, SM, RM and IM all differ in their method of excitation as well as in their operational behavior. In SMs the excitation field is built by permanent magnets or by a DC rotor current. This field has a fixed position within the rotor leading to a synchronous operation. RMs follow the principle of the reluctance forces and need no excitation field in the rotor. permanent magnet assistant synchronous reluctance machines (PSynRMs) combine the principle of the SM and the RM. The IM utilized the principle of induction to create an excitation field in the rotor. As a result, depending on the type of the machine various methods are used for the FE simulation which leads to different advantages and disadvantages. The different methods are shown in Fig. 9. For DC machines, SMs and RMs the static FEA is conducted. For the IM the transient FEA is used to consider the induction principle and the built-up of the rotor flux.

The modeling of SMs as well as of RMs or PSynRMs is performed in a rotor flux dq-reference frame, that includes saturation and magnetic cross coupling [31].
During the simulation the quadrature and direct current are varied and the torque can be calculated for those different excitations by methods like the eggshell method [32].
In Fig. 10 the calculated torque and flux-linkage for different dq-current excitations of an exemplary simulated SM is shown. Due to a constant stator current frequency during the machine simulation the iron losses are, in a first step, calculated for this certain frequency. In a second step, this frequency and therefore those iron losses are scaled according to the speed of the machine. To transfer the simulated operating points in the torque speed operating map of the machine different control strategies are used [3]. In the base speed range the Minimum-Torque-Per-Ampere (MTPA) and for the field weakening range the Minimum-Torque-Per-Flux (MTPF) control strategies are used. The calculation and scaling of the iron losses is described at the end of this section.

In contrast to the SM the IM utilized the principle of induction to create an excitation field in the rotor. To simulate the

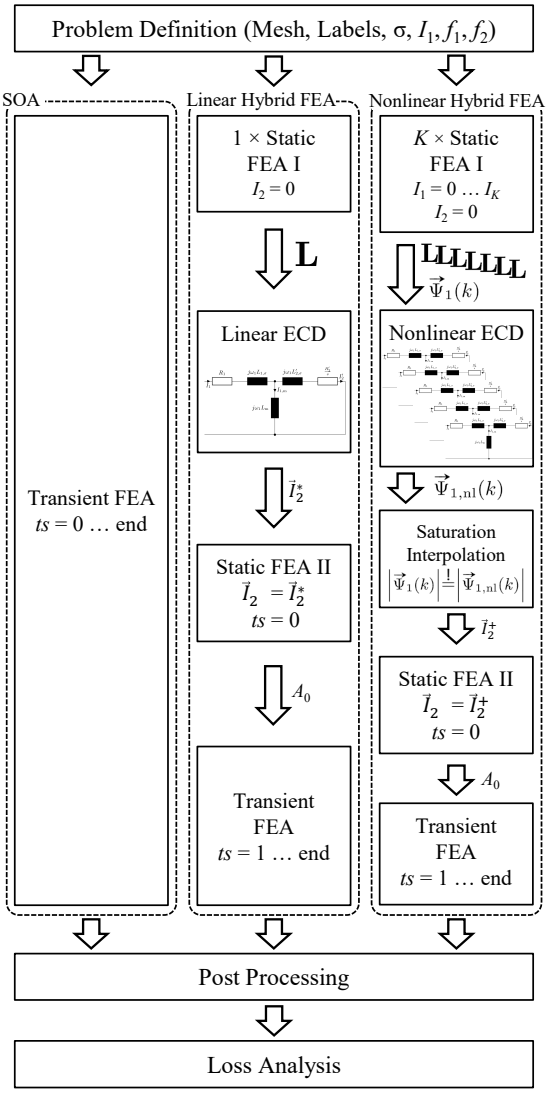

Fig. 9. FE simulation methods [24].

rotor flux build-up of an IM the transient FEA is conducted. This method is the state of the art for IM. Depending on the rotor time constant of the machine the flux build-up of the IM with the transient FEA leads to a very time consuming simulation [33] compared to the static FEA of SMs. To shorten the flux development at the IEM additional simulation approaches are available (Fig. 9). In the linear and nonlinear hybrid FEA transient and static FE simulations are coupled with analytic models resulting in a hybrid simulation scheme. In [24] it is shown, that those approaches reduce the simulation time of the IM, especially of the rotor flux development drastically. One requirement for this hybrid simulation scheme is the extraction of the lumped parameter matrices L and R describing the inductances and resistances described in [34]. A further contrast to the simulation of the SM is, that the IM is not simulated in the rotor flux dq-reference frame. According to [33] all reactances and the transformed rotor resistance $R_2^{'}/s$ are proportional to the stator frequency

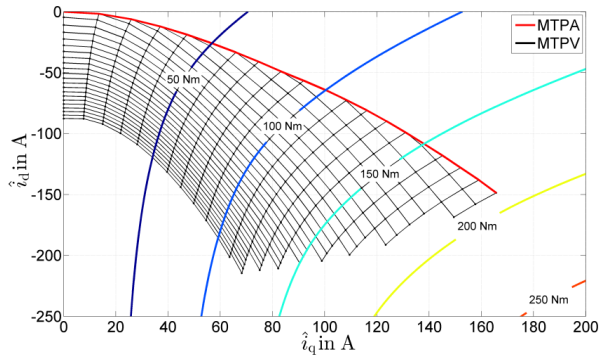

Fig. 10. Mesh of operating points with the calculated torque and flux-linkage of a SM [3].

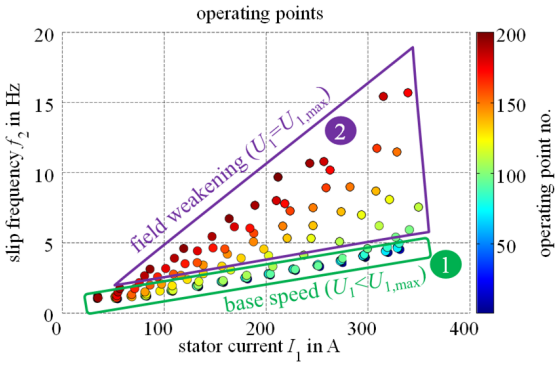

Fig. 12. Operating points of an IM in the $I_1 - f_2 -$ map [33].

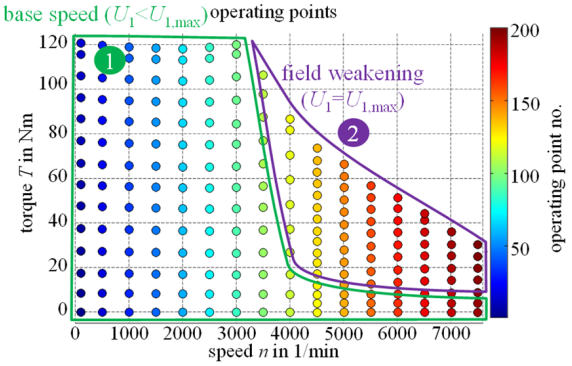

Fig. 11. Operating points of an IM in the $T - n -$ map [33].

ω_1. As a result the current allocation of the stator current I_1 into the magnetizing current I_μ and rotor current $I_2^{'}$ is independent on the stator current frequency. By subtracting the voltage drop over the stator resistance this allocation can be determined by the stator current itself, the rotor current frequency f_2 and the saturation of the main inductance. With this knowledge the operating points in terms of torque speed operating points, shown in Fig. 11, can be mapped in a stator current - rotor current frequency plane, shown in Fig. 13. The stator current−rotor current frequency−map ($I_1 - f_2 -$ map) is also used as the mesh grid for the IM FE simulation. As for the SM simulation the stator frequency is constant during the simulation of the IM. The iron losses are also calculated, in a first step, with the constant frequency and are scaled, in a second step, according to the speed.

1) Ohmic loss calculation: The Ohmic losses in the three phase stator are calculated by

$$P_{\mathrm{Ohmic},1} = 3 \cdot R_{1,20} \cdot (1 + \alpha_{20} (\vartheta - \vartheta_0)) \cdot I_1^2, \qquad (21)$$

with the stator resistance at 20 °C $R_{1,20}$, the temperature coefficient α_{20}, the reference winding temperature ϑ_0 and the simulated winding temperature ϑ.
For the IM the Ohmic losses in the rotor bars have to be considered. The current density value of each FE area $J_{2,\mathrm{i}}$ is calculated by the multiplication of the conductivity σ_2 of the bar material and the time derivative of the magnetic vector potential $\vec{A}_\mathrm{i}$:

$$J_{2,\mathrm{i}} = \sigma_2 \cdot \frac{\partial \vec{A}_\mathrm{i}}{\partial t}. \qquad (22)$$

For every time step the rotor Ohmic losses $p_{\mathrm{Ohmic},2}(t)$ are calculated as the sum of the rotor Ohmic losses in each rotor bar element with the element crossing area $A_{\mathrm{EL,i}}$ and the active iron length l_{Fe}:

$$p_{\mathrm{Ohmic},2}(t) = \sum_\mathrm{i} \frac{1}{\sigma} \cdot J_{2,\mathrm{i}}^2 \cdot A_{\mathrm{EL,i}} \cdot l_{\mathrm{FE}}. \qquad (23)$$

The average Ohmic rotor losses $P_{\mathrm{Ohmic},2}$ are calculated with

$$P_{\mathrm{Ohmic},2} = \frac{1}{T} \sum_{t=t_0}^{t_0+T} p_{\mathrm{Ohmic},2}(t), \qquad (24)$$

where T is the period length. This calculation method considers different local current distribution due to the skin or proximity effect.

2) Iron loss calculation: As described in section IV the total iron losses of a electric machine can be described by the IEM formula (15). However, the design and the operation of rotating electrical machines leads to a distortion of the fundamental waveform of the magnetic flux density [35]. In addition the fundamental waveform of the magnetic flux density is influenced by other effects, such as the saturation of the iron, the skin effect in the stator or rotor conductors and the use of power electronic supply in form of inverters and pulse width modulation (PWM) technique. Rotating vector magnetic fields can occur inside the magnetic core leading to so called rotational iron losses. To consider this rotational losses and the high harmonic losses an iron loss calculation in the frequency domain is performed. To identify the harmonics of the magnetic flux density a Fourier analysis is utilized. The level of the magnetic flux distortion and also the magnetic saturation can be considered with two parameters, $B_{\min}$ and $B_{\max}$ respectively. $B_{\min}$ describes the minimum and $B_{\max}$ the maximum magnetic flux density amplitude over one electrical period and therefore, with both parameters the locus of the magnetic flux density is described. The ratio between $B_{\min}$

and $B_{\max}$ defines the level of the magnetic flux distortion. In addition, the parameter $B_{\max}$ is an indicator for the saturation level. The hysteresis losses, calculated with parameter a_1, are effected by rotational magnetization. The eddy current losses, calculated with parameter a_2, are influenced by higher harmonics in the flux density. The excess losses, calculated with parameter a_3, are influenced by both effects, the rotational magnetization and the higher harmonics. To include these effects the loss contribution in the IEM formula (15) is extended to [35]:

$$P_{\mathrm{hyst}} = a_1 \cdot \sum_{n=1}^{\infty} \left(\left(B_{n,\mathrm{x}}^2 + B_{n,\mathrm{y}}^2 \right)^{\frac{\alpha}{2}} \cdot nf \right), \tag{25}$$

$$P_{\mathrm{cl}} = a_2 \cdot \left(\sum_{n=1}^{\infty} \left(B_{n,\mathrm{x}}^2 + B_{n,\mathrm{y}}^2 \right) \cdot (nf)^2 \right) \tag{26}$$

$$P_{\mathrm{exc}} = a_5 \cdot \left(1 + \frac{B_{\min}}{B_{\max}} \cdot \left(r_{\mathrm{exc}} \left(B_{\max} \right) - 1 \right) \right) \cdot \left(\sum_{n=1}^{\infty} \left(B_{n,\mathrm{x}}^2 + B_{n,y}^2 \right)^{0.75} \cdot (nf)^{1.5} \right) \tag{27}$$

$$P_{\mathrm{nl}} = a_2 \cdot a_3 \cdot B_{\max}^{2+a_4} \cdot f^2, \tag{28}$$

where n is the order of the harmonic, f the fundamental frequency, B_{x} and B_{y} the magnetic flux density in radial and tangential direction and r_{exc} an additional loss parameter of the excess losses. The parameter P_{nl} describes the non linear losses. This iron loss model (25) to (28) is validated in [36] and used in the FE model of the SM.

For IM, similar to the SM, the stator current frequency f_1 is in a range between $50\,\mathrm{Hz}$ up to $1500\,\mathrm{Hz}$. High stator frequencies lead to a significant influence of flux pulsations in rotor and stator teeth. This slotting frequencies can achieve values up to multiple kilohertz [33] and have an impact on the iron losses. To prevent sub sampling and aliasing of the magnetic flux pulsation in the teeth from the slotting harmonics, a sampling frequency of several thousand Hertz is necessary. This results in a small simulation time step. In contrast to this high frequencies of the slotting harmonics the fundamental rotor current frequency f_2 of an IM is, with $0\,\mathrm{Hz}$ to $16\,\mathrm{Hz}$, depending on the operating point, small. In the case that time harmonic formulations are used to calculate the iron losses, as it is done for the SM, a minimum period of $T_{\min} = \frac{1}{f_2}$ has to be simulated to cover one full magnetization period. For a rotor current frequency of $1\,\mathrm{Hz}$ the minimum time period is $T_{\min} = 1\,\mathrm{Hz}$. This high simulation time period in combination with the high sampling frequency to cover the slotting harmonics leads to multiple thousand time steps per simulation resulting in an inadequately high computational effort [33]. To avoid this high computational effort, the iron loss calculation can be performed in the time domain instead of the frequency domain. Therefore, transient formulations of the hysteresis losses (30), the macroscopic Foucault eddy current losses (31) and the microscopic excess losses (32) are used according to [37]. The sum of all three iron loss parts results in the total iron losses:

$$p_{\mathrm{iron}}(t) = p_{\mathrm{hyst}}(t) + p_{\mathrm{cl}}(t) + p_{\mathrm{exc}}(t). \tag{29}$$

The instantaneous hysteresis loss density $p_{\mathrm{hyst}}(t)$ in $\mathrm{W/kg}$ is calculated by the specific density of the specific material ρ, the irreversible magnetic field strength H_{irr} and the time differential of the magnetic flux density in radial and tangential direction, $\frac{\mathrm{d}B_{\mathrm{r}}}{\mathrm{d}t}$ and $\frac{\mathrm{d}B_{\vartheta}}{\mathrm{d}t}$ respectively. The Foucault eddy current and the excess loss density are described by the time differential of the magnetic flux densities in each direction and the material dependent loss factor k_{cl} and k_{exc}:

$$p_{\mathrm{hyst}}(t) = \rho \cdot \left(\left\| H_{\mathrm{irr}} \frac{\mathrm{d}B_{\mathrm{r}}}{\mathrm{d}t} \right\| + \left\| H_{\mathrm{irr}} \frac{\mathrm{d}B_{\vartheta}}{\mathrm{d}t} \right\| \right) \tag{30}$$

$$p_{\mathrm{cl}}(t) = k_{\mathrm{cl}} \frac{1}{2\pi^2} \cdot \left(\left\| \frac{\mathrm{d}B_{\mathrm{r}}}{\mathrm{d}t} \right\|^2 + \left\| \frac{\mathrm{d}B_{\vartheta}}{\mathrm{d}t} \right\|^2 \right) \tag{31}$$

$$p_{\mathrm{exc}}(t) = k_{\mathrm{exc}} \frac{1}{8.763} \cdot \left(\left\| \frac{\mathrm{d}B_{\mathrm{r}}}{\mathrm{d}t} \right\|^2 + \left\| \frac{\mathrm{d}B_{\vartheta}}{\mathrm{d}t} \right\|^2 \right)^{0.75} \tag{32}$$

In [37] the static hysteresis loop is approximated by an equivalent ellipse, that is described by:

$$H_{\mathrm{irr}}(B, B_{\max}) = \frac{k_{\mathrm{hyst}} \cdot B_{\max}}{\pi \cdot \rho} \cos\left(\arcsin\left(\frac{B}{B_{\max}} \right) \right), \tag{33}$$

with the maximum absolute flux density that is reached in the history of the material $B_{\max}$, the actual absolute magnetic flux density B and the hysteresis loss factor k_{hyst}. The hysteresis loss parameter k_{hyst} and the excess loss parameter k_{exc} are determined by magnetic measurements.The eddy current loss factor k_{cl} is calculated using the thickness of the steel sheet d, the specific electrical resistivity ρ_{e} and ρ as given [37]:

$$k_{\mathrm{cl}} = \frac{\pi^2 d^2}{6 \cdot \rho \rho_{\mathrm{e}}}. \tag{34}$$

3) Scaling of the iron losses and the FE simulation results: To obtain the efficiency map of the SM or IM the solutions of the FE simulation have to transformed into the $T - n -$ map by using control strategies, such as MTPA and MTPF, and by scaling the losses. Both the SM and the IM are simulated for a constant stator frequency. Therefore, the iron losses of the machines have to be scaled for different speeds and frequencies respectively. The different iron loss components of the stator and rotor are scaled according to:

$$p_{\mathrm{hyst}} \propto n, \tag{35}$$

$$p_{\mathrm{cl}} \propto n^2 \text{ and} \tag{36}$$

$$p_{\mathrm{exc}} \propto n^{1.5}. \tag{37}$$

This approach is sufficiently precise as described in [33].
Besides the scaling of the iron losses due to different speeds further scaling methods and approaches are used in the electromagnetic design process of the machine. In [38] scaling methods to the scale SM in radial and axial dimensions as well

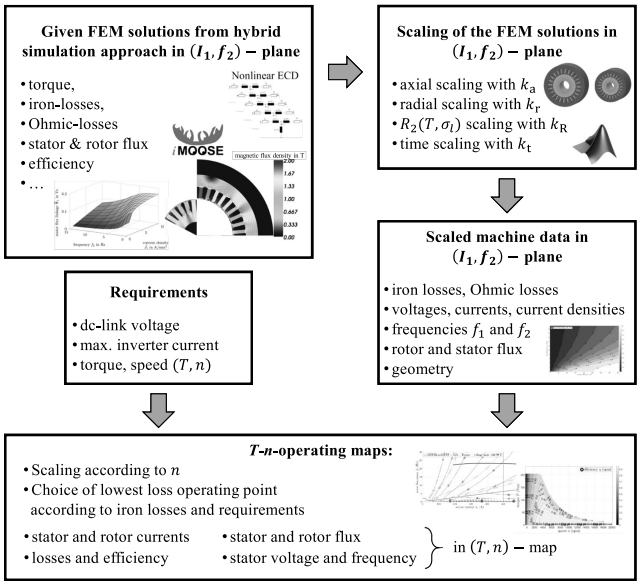

Fig. 13. Post processing process of an FE simulation of an IM [39].

as to rewind it in the post processing of the FEM are proposed. The IEM also developed a scaling approach to scale the FE solutions of an IM [39]. With this approach a radial and axial scaling, a rewinding and a scaling of the rotor resistance due to changes in the conductivity or geometry of the rotor bars in the post processing step are possible. The entire described process of the FEM post processing is shown in Fig. 13.

VI. Mechanical simulation

In the mechanical simulation, not only production but also operating influences on mechanical stresses can be considered. The most significant mechanical load caused by machine operation in high speed application is the centrifugal load [40]. In the mechanical simulation tool, the local deformation and the principal stresses are calculated for the rotor and extracted in dependency of the location. For the electromagnetic simulation, the deformed rotor geometry must be combined with the stator of the machine and is meshed triangularly. Then, the electromagnetic simulation is performed. The mechanical stress distribution is transferred to the electromagnetic machine model. For each element, the information of the mechanical stress in the element's center is provided. With the knowledge of the mechanical stress distribution inside the machine, the magneto-elastic effect can be implemented. In the simulation, the relative magnetic permeability is provided locally as a function of the mechanical uniaxial stress and the magnetic flux density via stress-dependent material data. This data is extracted from the measurement results presented in [41]. With knowledge of the magnetic flux density distribution, the machine properties, average torque and iron losses in the rotor can be determined.

1) Centrifugal force simulation: The mechanical static stress distribution caused by centrifugal forces inside a rotating disc can be estimated by calculating the in-plane stress components (σ_r: radial component and σ_t: tangential component) of a disc with a concentric bore diameter:

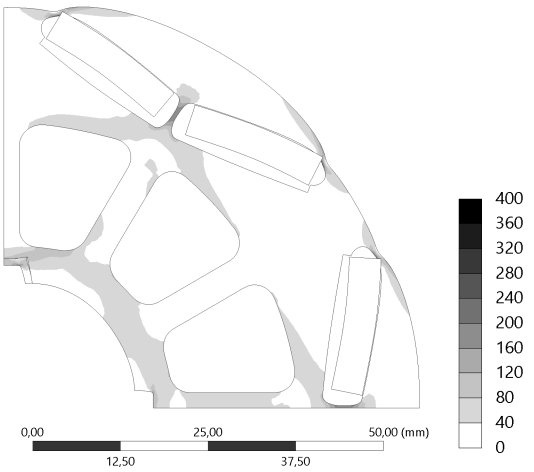

Fig. 14. Mechanical stress distribution in MPa for $n = 12\,000\,\mathrm{min}^{-1}$.

$$\sigma_r = (3+\nu)\frac{\rho\omega^2}{8}\left(r_1^2 + r_2^2 - \frac{r_1^2 r_2^2}{r^2} - r^2\right) \text{ and} \tag{38}$$

$$\sigma_t = (3+\nu)\frac{\rho\omega^2}{8}\left(r_1^2 + r_2^2 - \frac{r_1^2 r_2^2}{r^2} - \frac{1+3\nu}{3+\nu}r^2\right). \tag{39}$$

ν is the Poisson's ratio, ρ the material density, ω the speed and r_1 and r_2, the inner or outer radius, respectively.

Using the von-Mises criteria when shear stresses are neglected the stress distribution:

$$\sigma_{vM} = \sqrt{\sigma_r^2 + \sigma_t^2 - \sigma_r \sigma_t} \tag{40}$$

can be calculated. In rotors of SM, the stress distribution is influenced by the geometry. The position and size of the magnet pockets affect the stress distribution as well as additional cut outs or the shaft-hub joint (notches or stress caused by shrink fitting).

In Fig. 14, the simulated von-Mises stress distribution inside the rotor lamination of a SM for different magnet arrangements at the maximum rotor speed of $12\,000\,\mathrm{rpm}$ is shown. The stress distribution is mainly influenced by the magnet arrangement. The lowest resulting stress is produced when using glued magnets inside the rotor pockets. The highest stress results for unglued magnets. Due to the centrifugal forces, the unglued magnets are pushed against the outer pocket edge and cause a high load between pocket and rotor edge.

2) Structural dynamics: Acoustic machine aspects in motor development are becoming more important [42]. The characteristics of radiated airborne sounds are influenced by the combination of the structural dynamic characteristics of the motor and its force excitation. Therefore the determination of modal parameters by means of a modal analysis is a key aspect of the vibro-acoustic simulation and validation chain [43].

The quality of a numerical modal analysis depends on the accuracy of the models used to describe the material properties

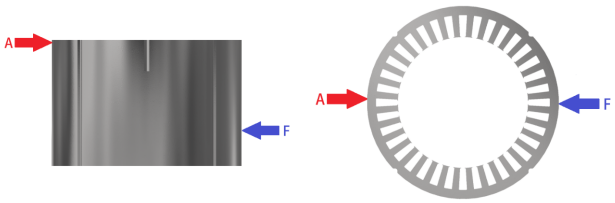

Fig. 15. Stator geometry and exemplary measurement points.

of the rotor and stator cores. Different packaging methods of rotor and stator cores require dedicated material models to take the varying stiffness, weight and damping parameters into account.

Experiments are conducted to examine the behavior of baked and welded cores and develop adequate material models. Stators with identical geometry but differing lamination techniques serve as test objects. The experiments are conducted at the IEM's modal analysis test bench. The stators are placed in the test area with elastic supports to minimize the effect of support structure on the modal behavior of the test objects. In this way a so called free-free boundary condition is approximately achieved. The stators are excited using a modal hammer with a force sensor in its tip and the structural response is measured by means of acceleration sensors. The frequency response function (FRF) between the excitation and the measurement point can thus be calculated with the formula [44]:

$$A(\omega) = \frac{A}{F}, \tag{41}$$

where A represents the measured acceleration response in frequency domain and F represents the measured excitation force in frequency domain. Integrating the FRF two times yields the receptance [44]:

$$H(\omega) = \frac{1}{\omega^2}\frac{A}{F} = \frac{X}{F}. \tag{42}$$

Measuring the acceleration response at multiple locations allows the calculation of multiple receptances from which modal parameters can be extracted. To extract the modal parameters, eigenfrequencies, mode shapes and modal damping ratios, the data are evaluated with the 3 dB method [44], the Circle-Fit method [44], the Rational-Fraction-Polynomial method [45] as well as the Least-Squares-Rational-Fit method [46].

Fig. 16 and 17 show the extracted mode shapes at their respective eigenfrequencies. Further examination of the data yields the modal damping ratios as shown in table I and table II. A comparison between a baked and a welded core shows, that modes which exhibit shear deformation appear at lower eigenfrequencies in the modal analysis of the welded core and have higher modal damping ratios, than in the baked core. Modes without shear remain at about the same eigenfrequencies when comparing the stators to each other and exhibit similar damping values. The material model of the

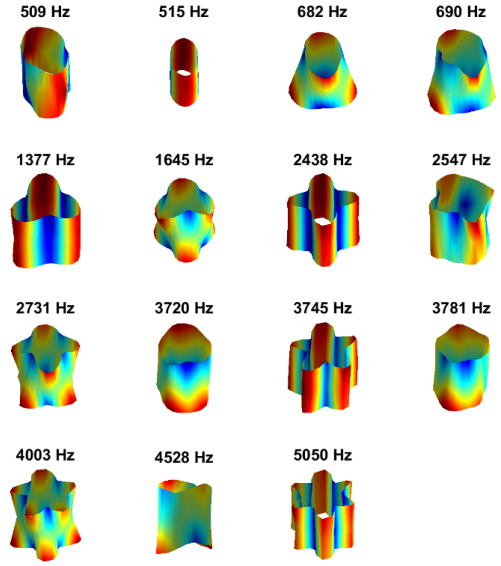

Fig. 16. Measured mode shapes of the baked stator core.

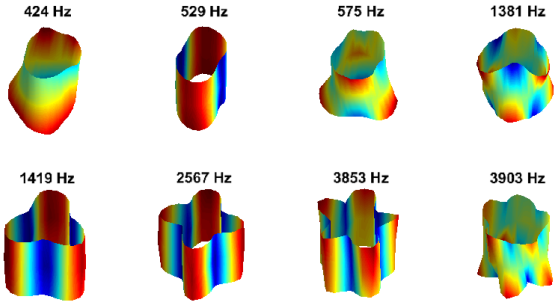

Fig. 17. Measured mode shapes of the welded stator core.

numeric simulation has to take these manufacturing method induced characteristics into account.

A homogeneous, anisotropic material model according to [47] is used to simulate the baked core and modified to accurately describe the properties of the welded core. As FE simulations with these homogeneous material models show, the lowered eigenfrequencies of modes with shear deformation

TABLE I
CALCULATED MODAL DAMPING RATIOS OF THE BAKED CORE.

Eigenfrequencies	Damping Ratio
509 Hz	0.0003
682 Hz	0.0022
1377 Hz	0.0004
1645 Hz	0.0019
2438 Hz	0.0004
2731 Hz	0.0018
3720 Hz	0.0045
3745 Hz	0.0007
4003 Hz	0.0015
4528 Hz	0.0045
5050 Hz	0.0006

TABLE II
CALCULATED MODAL DAMPING RATIOS OF THE WELDED CORE.

Eigenfrequencies	Damping Ratio
424 Hz	0.0213
529 Hz	0.0001
575 Hz	0.0507
1381 Hz	0.0413
1419 Hz	0.0004
2567 Hz	0.0005
3853 Hz	0.0006
3903 Hz	0.0098

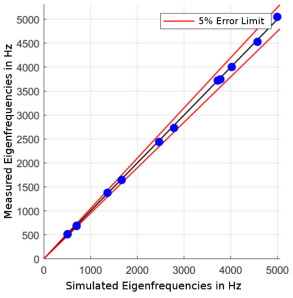

Fig. 18. Eigenfrequency comparison between simulation and measurement of the baked core.

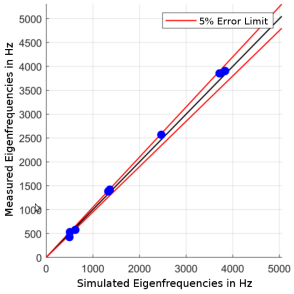

Fig. 19. Eigenfrequency comparison between simulation and measurement of the welded core.

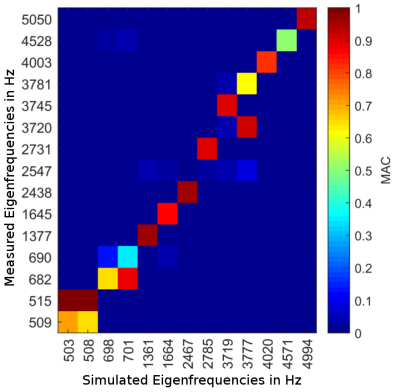

Fig. 20. MAC matrices of the baked core.

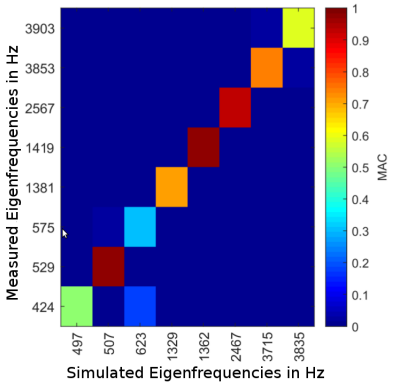

Fig. 21. MAC matrices of the welded core.

can be attributed to the lower homogeneous shear modulus of the welded cores. The higher damping of modes with shear deformation in the welded stator is attributed to friction losses between the metal sheets. The modal damping values in the baked stator show a similar behavior. Modes with shear deformation have higher damping values than those without, which be explained by the higher damping of baking varnish when compared to steel. The damping caused by friction between the metal sheets is higher than the damping caused by baking varnish.

The structural dynamic behavior can be simulated by conducting a numerical modal analysis with a free-free boundary condition. This simulation yields the eigenfrequencies and the mode shapes of the structure. A subsequent harmonic analysis can be used to simulate receptances. Measured damping ratios can be taken into account in the harmonic analysis. model assurance criterion (MAC) matrices are used to assess the quality of the numerical modal analysis [48]. Fig. 20 and 21 show the MAC matrices, which validate the mode shapes of the FE model. The validity of the simulated eigenfrequencies is shown in a comparison between simulated and measured eigenfrequencies in Fig. 18 and 19. The validated FE model opens up the possibility to predict changes in eigenfrequencies and mode shapes, when the geometry or material parameters change without having access to a physical prototype of the modified structure.

VII. CONTROL / POWER ELECTRONICS

With the high level of maturity that electric machines have reached, the further advancing power electronics and the increasingly faster control systems, the potential for improvement on the system level, rather than component level, shifts more into focus. The development of control systems and electronics which takes the behavior of the electrical machines and even complete drive trains into account requires fast yet accurate models. Simulation on system level allows for example to improve the machine dynamics or noise emission via optimized control strategies, analyze the impact of new transistors capable of higher switching frequencies or get a deeper understanding of the impacts of production deviations.

The very short minimum closed times of the power electronics require for short simulation time steps for them to be accurately simulated, especially if the switching process itself has to be resolved. On the other hand the physical effects which determine the machine behavior heavily depend on the machine geometry and the electromagnetic status, which requires an accurate but time-consuming model. To match both requirements a hybrid approach from [49], [50] is used combining an analytical lumped parameter model with the advantages of the shown finite element method. The lumped parameters are calculated in advance for every machine status in independent FE simulations, which can be executed massively parallel on modern multi-CPU workstations or clusters. The parameters are gathered in maps, with the dimensions flexibly depending on the problem. In addition to saturation state and slotting effect, this approach allows for the analysis further

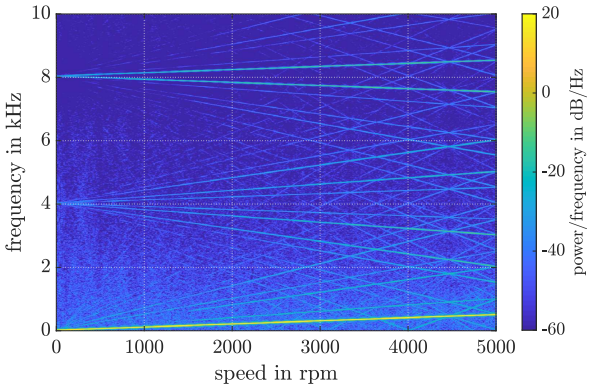

Fig. 22. Simulated phase current on run up with 4 kHz PWM frequency.

effects such as rotor eccentricity or production deviations. The application of the multi slice method from [51], [52] on the current calculation is presented in [53] to represent skewing, torsion, and, in combination with eccentricity, bending and rotor vibrations. The electromagnetic forces, which can also be acquired from the FEA, and the position depended lumped parameter are the basis for a strong coupling with structural dynamic models. Fig. 22 shows a simulated phase current with an IGBT model and 4 kHz PWM frequency.

VIII. Thermal Simulation

The request for high power density electrical motors in traction applications leads to a higher amount of heat that needs to be dissipated from a limited volume. A maximum admissible heat dissipation at critical components must be ensured [21], [54]. For the improvement of heat dissipation in electric machines, several cooling technologies are discussed in literature. A review is given in [55].

1) Thermal models: Different numerical models for thermal simulation of electric machines can be used. In general there is a trend towards increasing accuracy when the number of nodes and the model complexity is increased. Particularly for thermal problems, this trend is not generally valid as the model accuracy is significantly influenced by component interfaces, material characteristics and boundary conditions of the simulation problem. As these influencing factors are often unknown, a selection of a proper simulation model needs to be adjusted to the available system information and measurement data. In the following section, different models are introduced and discussed starting with low complexity models.

A frequently used low complexity model is a reduced order lumped parameter model such as a three node model. An example of such a model is depicted in Fig. 23.

The temperatures can be evaluated for the three nodes, i.e. the rotor T_r, the stator winding $T_\mathrm{s,Cu}$ and the stator iron $T_\mathrm{s,Fe}$. Losses such as the rotor losses P_r can be introduced. The capacities of all motor components are cumulated in the three capacities C_i. The resistance R between the nodes need to be identified. A combination of analytical formula and test bench measurements is possible for the parameterization of the model, whereas second approach is indispensable. Due to this need, the model cannot be used for completely new electric

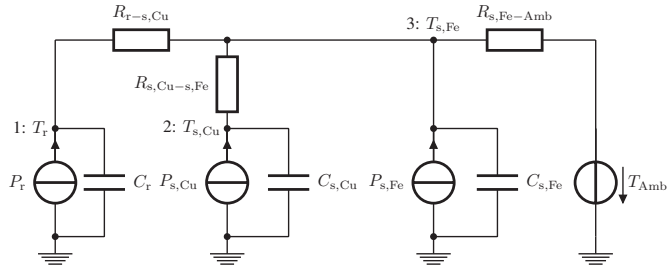

Fig. 23. Thermal four node model of an electrical machine.

machine cooling designs. Fields of application are simulation of entire drive units or sensitivity studies like shown in [56].

In a high order lumped parameter model, the number of nodes is increased and each thermal processes is described by analytical formula. The model is well suited for description of the entire motor and thus it is the state of the art model that is used for a new design of an electrical machine [54], [57].

For detailed problems which are driven by heat conduction such as the thermal behavior in the winding, FEA is used. As an example, the results of a two dimensional FEA of a stator slot for a traction drive is depicted in Fig. 24. Using the FEA, the location and temperature of the hot spot in the winding can be determined. The influence of the impregnation material as well as the location of the conductors can be studied. Further, the results of the FEA can be used to parameterize resistances for the high order lumped parameter model that is used for the calculation of the entire drive train as shown in [58].

In order to simulate detailed thermal problems, where a fluid flow with heat conduction is present, a computational fluid dynamics (CFD) simulations can be used. Fields of research in electric machine design are the investigation of cooling channels, the heat transfer in the airgap or simulations of the end space [59]. The results of the CFD again can be used to parameterized a high order lumped parameter model.

2) Coupling of electromagnetic and thermal calculation: After finishing the calibration of the lumped parameter model, the model can be used to investigate the thermal behavior of the electric machine and different cooling methodologies in a $T-n-$map. As an example, the maximum stator temperature $T_\mathrm{stat} = 180\,^\circ\mathrm{C}$ is added in Fig. 25 to the efficiency plot in

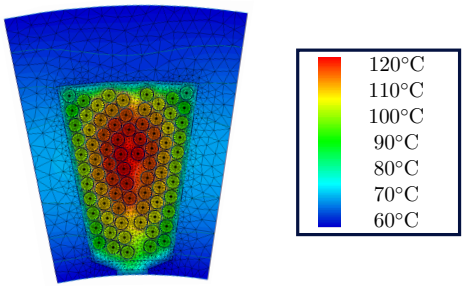

Fig. 24. Temperature distribution in the stator slot calculated with two dimensional FEA.

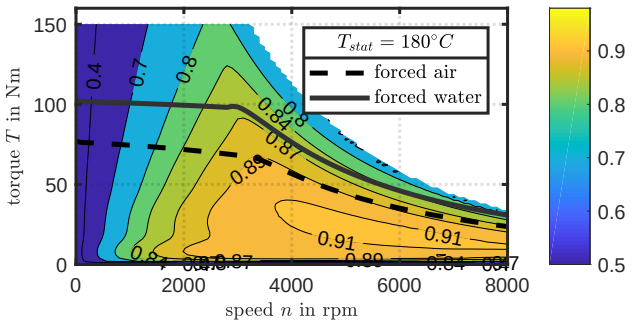

Fig. 25. Motor efficiency and operational limits for maximum stator temperature of $T_{\mathrm{stat}} = 180\,^{\circ}\mathrm{C}$.

the $T - n -$ map.

The maximum temperature represents the operational limit for continuous operation of the IM with different cooling methodologies, i.e. a stator cooling with forced air on the housing and a forced flow of a 50/50 mixture of ethylene glycol and water (EGW 50/50) around a helix formed cooling channel in the housing. The improved stator cooling methodology with EGW 50/50 leads to a significant improvement in the continuous operational limit for a small speed of the motor. In this area, copper losses are dominant and the heat extraction in the housing is close to the source and effective. For operational points at higher frequencies, iron losses play a more significant role. Here, an improved stator cooling is less effective as the heat transition paths within the machine play a more significant role.

IX. Conclusions

Designing and modeling a complete electric drive system is a complex process. In this paper a numerical complete modular computation scheme for an accurate multi-coupled electric drive systems has been presented. It starts with the rough design process and the principles of FE models. Here, the characterization and modeling of the material as well as the structure of the FEM solvers are outlined. The process of electromagnetic simulations for single operation points and for the calculation of the whole operation range of the machine are discussed in detail. The paper concludes with an insight into the mechanical simulations, considering centrifugal force simulations and structural dynamics as well as the thermal design and simulation of the electrical machine. The presented simulation scheme is modular being able to focus on individual effects with various levels of detail enabling a application specific design and simulation process. Many examples which can be taken from the exhausting attached list of publications confirm the usefulness of the implemented overall simulation approach.

References

[1] K. Hameyer, S. Böhmer, I. Coenen, D. Eggers, M. Felden, D. Franck, M. Hafner, F. Henrotte, T. Herold, M. Hombitzer, E. Lange, P. Offermann, B. Riemer, and S. Steentjes, "The art of modelling Electrical Machines," *ICS Newsletter, International Compumag Society*, vol. 19, no. 2, pp. 3–19, July 2012.

[2] A. Pohlmann, M. Leßmann, A. Fritschi, T. Finocchiaro, U. Steinseifer, and K. Hameyer, "Experimental validation of the linear drive train for a total artificial heart system," *Mechatronics*, May 2012.

[3] A. Ruf, S. Steentjes, G. von Pfingsten, T. Grosse, and K. Hameyer, "Requirements on Soft Magnetic Materials for Electric Traction Motors," in *Conf. Proc. 7th international Conference on Magnetism and Metallurgy, WMM'16*, Rome, Italy, May 2016, pp. 111–128.

[4] M. Felden, P. Bütterling, P. Jeck, L. Eckstein, and K. Hameyer, "Electric vehicle drive trains: From the specification sheet to the drive-train concept," in *14th International Power Electronics and Motion Control Conference, EPE/PEMC*. Ohrid, Macedonia: EPE-PEMC Council, September 2010, pp. 9–16.

[5] S. Böhmer, E. Lange, and K. Hameyer, "Non-conforming Sliding Interfaces for Motion in 3D Finite Element Analysis of Electrical Machines by Magnetic Scalar Potential Formulation Without Cuts," in *15th Biennial IEEE Conference on Electromagnetic Field Computation, CEFC 2012*. Oita, Japan: Institute of Electrical and Electronics Engineers (IEEE), November 2012, p. 244.

[6] N. Leuning, S. Elfgen, H. A. Weiss, W. Volk, and K. Hameyer, "The influence of and an appropriate numerical model to simulate cut-edge effects of electrical steel laminations," in *presentation at moredrive 2019*. oVE akademie, January 2019.

[7] A. J. Moses, N. Derebasi, G. Loisos, and A. Schoppa, "Aspects of the cut-edge effect stress on the power loss and flux density distribution in electrical steel sheets," *Journal of Magnetism and Magnetic Materials*, vol. 215–216, pp. 690–692, Jun. 2000.

[8] A. Schoppa, J. Schneider, and C. D. Wuppermann, "Influence of the manufacturing process on the magnetic properties of non-oriented electrical steels," *Journal of Magnetism and Magnetic Materials*, vol. 215–216, pp. 74–78, Jun. 2000.

[9] N. Leuning, S. Elfgen, B. Groschup, G. Bavendiek, S. Steentjes, and K. Hameyer, "Advanced Soft- and Hard-Magnetic Material Models for the Numerical Simulation of Electrical Machines," *IEEE Transactions on Magnetics*, vol. 54, pp. 1–8, October 2018.

[10] S. Elfgen, S. Steentjes, S. Böhmer, D. Franck, and K. Hameyer, "Continuous Local Material Model for Cut Edge Effects in Soft Magnetic Materials," *IEEE Transactions on Magnetics*, vol. 52, no. 5, pp. 1–4, May 2016.

[11] N. Leuning, S. Elfgen, H. A. Weiss, W. Volk, and K. Hameyer, "The influence of and an appropriate numerical model to simulate cut-edge effects of electrical steel laminations," *e & i Elektrotechnik und Informationstechnik*, 2019.

[12] C. P. Steinmetz, "On the law of hysteresis," vol. 72, no. 2, pp. 197–221, 1984.

[13] N. Leuning, S. Steentjes, and K. Hameyer, "Effect of grain size and magnetic texture on iron-loss components in NO electrical steel at different frequencies," *Journal of Magnetism and Magnetic Materials*, vol. 469, pp. 373–382, October 2019.

[14] D. Eggers, S. Steentjes, and K. Hameyer, "Advanced iron-loss estimation for nonlinear material behavior," vol. 48, no. 11, pp. 3021–3024, 2012-11.

[15] S. Jacobs, F. Henrotte, M. Herranz Gracia, K. Hameyer, P. Goes, and D. Hectors, "Magnetic material optimization for hybrid vehicle PMSM drives." Avere, 2009.

[16] S. Steentjes, M. Leßmann, and K. Hameyer, "Semi-physical parameter identification for an iron-loss formula allowing loss-separation," vol. 113, no. 17, p. 17A319, 2013-05-07.

[17] J. Karthaus, S. Steentjes, N. Leuning, and K. Hameyer, "Effect of mechanical stress on different iron loss components up to high frequencies and magnetic flux densities," *COMPEL - The international journal for computation and mathematics in electrical and electronic engineering*, vol. 36, no. 3, pp. 580–592, 2017.

[18] A. Nouy, "A priori model reduction through proper generalized decomposition for solving time-dependent partial differential equations," *"Computer Methods in Applied Mechanics and Engineering"*, vol. 199, no. 23, pp. 1603 – 1626, 2010.

[19] S. Clénet and T. Henneron, "Error estimation for model-order reduction of finite-element parametric problems," *IEEE Transactions on Magnetics*, vol. 52, no. 8, pp. 1–10, Aug 2016.

[20] T. Henneron and S. Clénet, "Model order reduction of quasi-static problems based on pod and pgd approaches," *The European Physical Journal Applied Physics*, vol. 64, no. 2, p. 24514, 2013.

[21] A. Ruf, J. Paustenbach, D. Franck, and K. Hameyer, "A methodology to identify electrical ageing of winding insulation systems," in *2017*

IEEE International Electric Machines and Drives Conference (IEMDC). IEEE, 2017, pp. 1–7.

[22] A. Ruf, F. Pauli, M. Schröder, and K. Hameyer, "Lebensdauermodellierung von nicht-teilentladungsresistenten Isoliersystemen elektrischer Maschinen in dynamischen Lastkollektiven," *E & I Elektrotechnik und Informationstechnik*, vol. 2, pp. 131–144, March 2018.

[23] T. Finken, M. Hombitzer, and K. Hameyer, "Study and comparison of several permanent-magnet excited rotor types regarding their applicability in electric vehicles," in *Emobility - Electrical Power Train*. Leipzig, Germany: VDE, November 2010, pp. 1–7.

[24] G. von Pfingsten, M. M. Nell, and K. Hameyer, "Hybrid simulation approaches for induction machine calculation," *COMPEL - The international journal for computation and mathematics in electrical and electronic engineering*, 2018.

[25] M. Hombitzer, S. Elfgen, D. Franck, and K. Hameyer, "Performance improvement of a high-speed permanent magnet excited synchronous machine by flux-barrier design," in *XXI International Conference on Electrical Machines, ICEM 2014*. Berlin, Germany: IEEE, September 2014, pp. 1370–1376.

[26] B. Groschup, S. Elfgen, and K. Hameyer, "Local and Cut-Edge-Length Iron Loss Simulation Using a Local Material Model," in *Symposium on Electromagnetic Phenomena in Nonlinear Circuits, EPNC 2018*, Arras, Frankreich, June 2018.

[27] S. Elfgen, S. Steentjes, S. Böhmer, D. Franck, and K. Hameyer, "Continuous Local Material Model for Cut Edge Effects in Soft Magnetic Materials," *IEEE Transactions on Magnetics*, vol. 52, no. 5, pp. 1–4, May 2016.

[28] A. K. Putri, M. Nell, M. Hombitzer, D. Franck, and K. Hameyer, "On the design of a PMSM rotor with ferrite magnets to substitute a rare earth permanent magnet system," in *2018 XIII International Conference on Electrical Machines, ICEM18*, Alexandroupolis, Griechenland, September 2018.

[29] T.-C. Andrei, T. Kauder, J. Karthaus, M. Hombitzer, R. Appunn, and K. Hameyer, "Improved Rotor Pole Geometry of a PMSM for Wind Turbine Applications with Multiple High-speed Generators," in *Optimization of Electrical and Electronic Equipment (OPTIM)*, Brasov, Romania, May 2014, pp. 450–457.

[30] A. K. Putri, M. Hombitzer, D. Franck, and K. Hameyer, "Comparison of the Characteristics of Cost-Oriented Designed High-Speed Low-Power Interior PMSM," *IEEE Transactions on Industry Applications*, vol. 53, no. 6, pp. 5262–5271, November 2017.

[31] T. Herold, D. Franck, E. Lange, and K. Hameyer, "Extension of a D-Q Model of a Permanent Magnet Excited Synchronous Machine by Including Saturation, Cross-Coupling and Slotting Effects," in *International Electric Machines and Drives Conference, (IEMDC)*, Niagara Falls, Ontario, Canada, May 2011.

[32] F. Henrotte, G. Deliége, and K. Hameyer, "The eggshell approach for the computation of electromagnetic forces in 2D and 3D," *COMPEL*, vol. 23, no. 4, pp. 996–1005, 2004.

[33] G. von Pfingsten, S. Steentjes, and K. Hameyer, "Operating Point Resolved Loss Calculation Approach in Saturated Induction Machines," *IEEE Transactions on Industrial Electronics*, vol. 64, no. 3, pp. 2538–2546, March 2017.

[34] E. Lange, F. Henrotte, and K. Hameyer, "An Efficient Field-Circuit Coupling Based on a Temporary Linearization of FE Electrical Machine Models," *IEEE Transactions on Magnetics*, vol. 45, no. 3, pp. 1258–1261, March 2009.

[35] G. von Pfingsten, A. Ruf, S. Steentjes, and K. Hameyer, *Operation Mode Dependent Requirements on Magnetic Properties of NO Electrical Steel in Traction Drives*, ser. Tagungsband – Aachener Stahlkolloquium – Umformtechnik. Verlagshaus Mainz GmbH Aachen, Gerhard Hirt (Hrsg.), 2016, no. 1, pp. 163–176.

[36] S. Steentjes, G. von Pfingsten, M. Hombitzer, and K. Hameyer, "Enhanced iron-loss model with consideration of minor loops applied to FE-simulations of electrical machines," in *Joint MMM-Intermag*, Chicago, Illinois, USA, January 2013, p. 524.

[37] D. Lin, P. Zhou, W. N. Fu, Z. Badics, and Z. J. Cendes, "A dynamic core loss model for soft ferromagnetic and power ferrite materials in transient finite element analysis," *IEEE Transactions on Magnetics*, vol. 40, no. 2, pp. 1318–1321, March 2004.

[38] S. Stipetic, D. Zarko, and M. Popescu, "Scaling laws for synchronous permanent magnet machines," in *Tenth International Conference on Ecological Vehicles and Renewable Energies (EVER)*, March 2015, pp. 1–7.

[39] M. Nell, J. Lenz, and K. Hameyer, "Efficient numerical optimization of induction machines by scaled fe simulations," in *XIII International Conference on Electrical Machines (ICEM)*, Sep. 2018, pp. 198–204.

[40] J. Karthaus and K. Hameyer, "Static and cyclic mechanical loads inside the rotor lamination of high-speed pmsm," in *7th International Electric Drives Production Conference, EDPC*, Würzburg, Germany, 2017, pp. 78–83.

[41] J. Karthaus, M. Balluff, M. Schröder, M. Gerlach, and K. Hameyer, "Study on the effect of stator segmentation on the characteristics of an electrical vehicle traction drive," in *ICS Newsletter, International Compumag Society*, 2018, pp. 25(1):3–10.

[42] M. Wegerhoff, *Methodik zur numerischen NVH Analyse eines elektrifizierten PKW Antriebsstrangs*. Verlagsgruppe Mainz GmbH Aachen, 2017.

[43] M. Schwarzer, C. Zimmerling, E. Barti, M. Dannemann, R. Bochynek, and T. Bein, "Analytical prediction of the effective dynamic behaviour and the damping characteristics of laminated steel stacks as used in electric machines."

[44] D. J. Ewins, *Modal testing: theory and practice*. Research studies press Letchworth, 1984, vol. 15.

[45] N. M. M. Maia *et al.*, "Extraction of valid modal properties from measured data in structural vibrations," 1988.

[46] A. A. Ozdemir and S. Gumussoy, "Transfer function estimation in system identification toolbox via vector fitting," *IFAC-PapersOnLine*, vol. 50, no. 1, pp. 6232–6237, 2017.

[47] M. Van der Giet, K. Kasper, R. De Doncker, and K. Hameyer, "Material parameters for the structural dynamic simulation of electrical machines," in *XXth International Conference on Electrical Machines*, 2012, pp. 2994–3000.

[48] R. J. Allemang, "The modal assurance criterion–twenty years of use and abuse," *Sound and vibration*, vol. 37, no. 8, pp. 14–23, 2003.

[49] T. Herold, E. Lange, and K. Hameyer, "System simulation of a pmsm servo drive using field-circuit coupling," *IEEE Transactions on Magnetics*, vol. 47, no. 5, pp. 938–941, May 2011.

[50] T. Herold, D. Franck, E. Lange, and K. Hameyer, "Extension of a d-q model of a permanent magnet excited synchronous machine by including saturation, cross-coupling and slotting effects," May 2011.

[51] F. Piriou and A. Razek, "A model for coupled magnetic-electric circuits in electric machines with skewed slots," *IEEE Transactions on Magnetics*, vol. 26, no. 2, pp. 1096–1100, March 1990.

[52] S. Williamson, T. J. Flack, and A. F. Volschenk, "Representation of skew in time-stepped two-dimensional finite-element models of electrical machines," October 1994.

[53] M. Jaeger, S. Rick, and K. Hameyer, "Representation of skew in time-stepped two-dimensional finite-element models of electrical machines," September 2018.

[54] M. Jaeger, A. Ruf, K. Hameyer, and T. G.-v. Tongeln, "Thermal analysis of an electrical traction motor with an air cooled rotor," in *2018 IEEE Transportation and Electrification Conference and Expo (ITEC)*. Piscataway, NJ: IEEE, 2018, pp. 467–470.

[55] M. Popescu, D. A. Staton, A. Boglietti, A. Cavagnino, D. Hawkins, and J. Goss, "Modern heat extraction systems for power traction machines—a review," *IEEE Transactions on Industry Applications*, vol. 52, no. 3, pp. 2167–2175, 2016.

[56] B. Assaad, K. El kadri Benkara, G. Friedrich, S. Vivier, and A. Michon, "Reducing the complexity of thermal models for electric machines via sensitivity analyses," in *ECCE 2017*, I. E. C. C. &. Expo, Ed. Piscataway, NJ: IEEE, 2017, pp. 4658–4665.

[57] D. Staton, A. Bogliette, and A. Cavagnino, "Solving the more difficult aspects of electric motor thermal analysis in small and medium size industrial induction motors," *IEEE TRANSACTIONS ON ENERGY CONVERSION*, vol. 20, no. 3, pp. 620–628, September 2005.

[58] R. Wrobel, S. J. Williamson, J. D. Booker, and P. H. Mellor, "Characterizing the in situ thermal behavior of selected electrical machine insulation and impregnation materials," *IEEE Transactions on Industry Applications*, vol. 52, no. 6, pp. 4678–4687, 2016.

[59] G. L. Basso, J. Goss, Y. C. Chong, and D. Staton, "Improved thermal model for predicting end-windings heat transfer," in *ECCE 2017*, I. E. C. C. &. Expo, Ed. Piscataway, NJ: IEEE, 2017, pp. 4650–4657.